Supporting information

Graphene mesh as a hybrid electrode for foldable devices

Eun-Hyoung Cho[1], Mi-Jeong Kim[2], Hiesang Sohn[3], Weon Ho Shin[4], Jung Yeon Won[1], Youngsung Kim[1], Chan Kwak[2], Chang Seung Lee[1] and Yun Sung Woo[2,5]

[1] Platform Technology Lab., Samsung Advanced Institute of Technology, 120 Samsung-ro, Yeongtong-gu, Suwon-si, Gyeonggi-do 443-803, South Korea

[2] Inorganic Material Lab., Samsung Advanced Institute of Technology, 120 Samsung-ro, Yeongtong-gu, Suwon-si, Gyeonggi-do 443-803, South Korea

[3] Department of Chemical Engineering, Kwangwoon Univ., 20 Kwangwoon-ro, Nowon-gu, Seoul 01897, South Korea

[4]Energy Materials Center, Energy and Environment Division, Korea Institute of Ceramic Engineering and Technology, 101, Soho-ro, Jinju-si, Gyeongsangnam-do, 52851, South Korea

[5] Dept. of Advanced Materials Application, Korea Polytechnic, 398 Sujeong-ro, Sujeong-gu, Seongnam-si, Gyeonggi-do 13122, South Korea

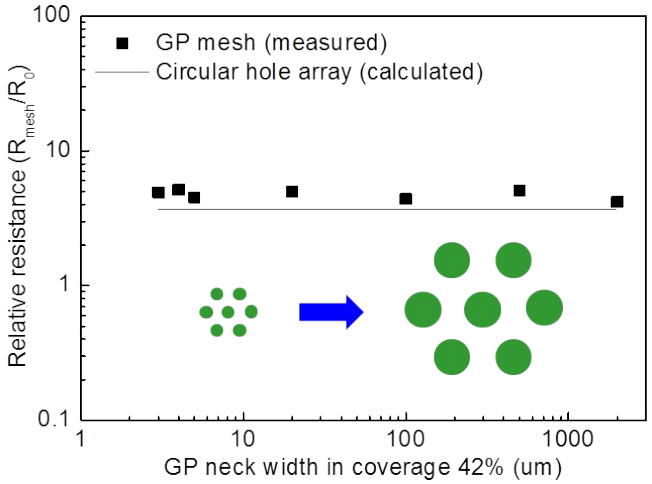

Fig. S1. Relative resistance of the GP mesh as a function of the neck width, maintaining 42% coverage. Thus, only the neck width and hole size are changed in our experiments. Note that the relative conductivity cannot be changed experimentally, if the coverage is consistent, regardless of the hole size. Note, because relative values are used in our simulations, the relative conductivity of the relative areal density does not depend on the material.

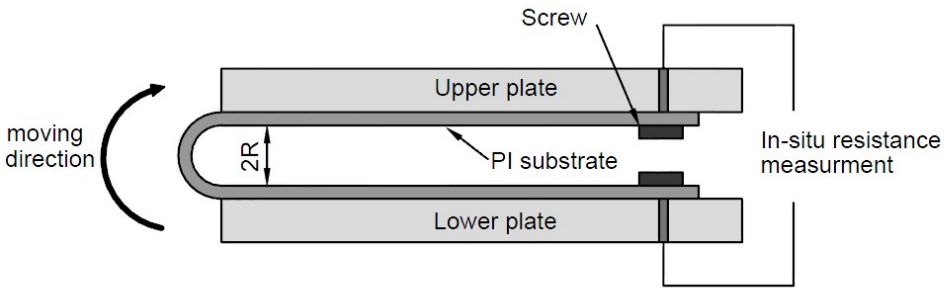

Fig. S2. Schematic of the cyclic bending test machine. The AgNW/GP hybrid film with an over coating layer on the PI fim is mounted in between the two parallel plates using screw bolts. Since the coated AgNW/GP film is located outside the folded PI substrate, the AgNW/GP film is subjected to repetitive tensile strain, and the tensile strain applied is determined by the thickness of the PI substrate and the distance between the two plates. The nominal strain imposed on the AgNW/GP for a given plate spacing is calculated to be $\varepsilon = y/R$, where y is the neutral plane which can be determined by the PI substrate thickness and R, the radius, which signifies a half-value of the distance between the plates. As shown in the above figure, the lower plate is fixed and the upper plate moves repeatedly from the horizontal position to the lower plate to the position corresponding to the given distance during repetitive bending.

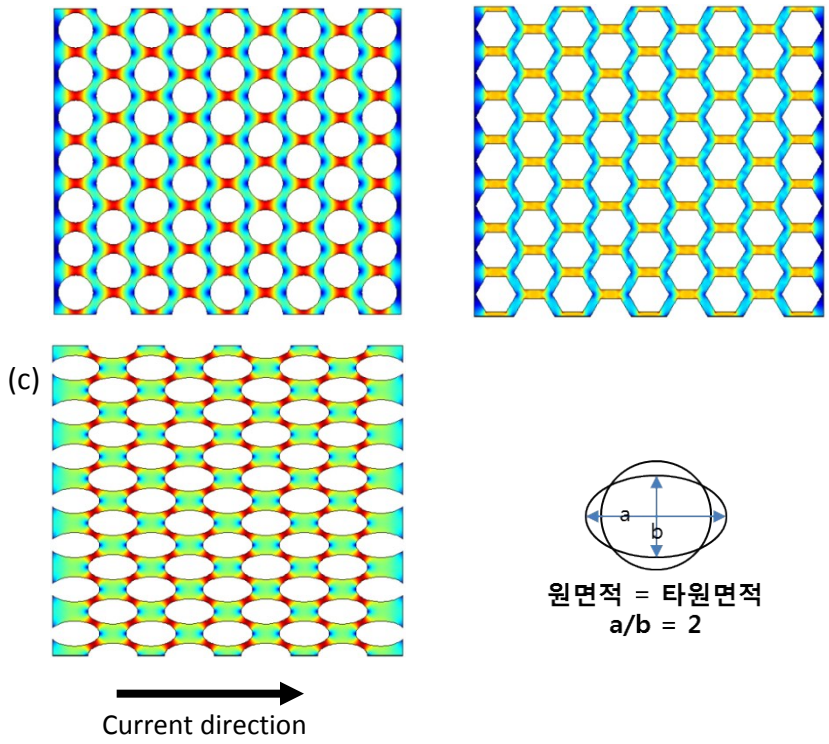

Fig. S3. The distribution of the electrical current density from FEM modeling for a mesh with a hexagonally arranged hole array with an areal density of 0.42. The mesh consists of (a) circular, (b) hexagonal, and (c) elliptical holes, and the distribution of the current density in the mesh varies greatly depending on the shape of the hole. Particularly, it can be seen that the disturbance of the current occurs at the narrowest part of the neck in the case of a mesh composed of an elliptic hole having the same area with the circular hole but the ratio of long and short axis of 2.

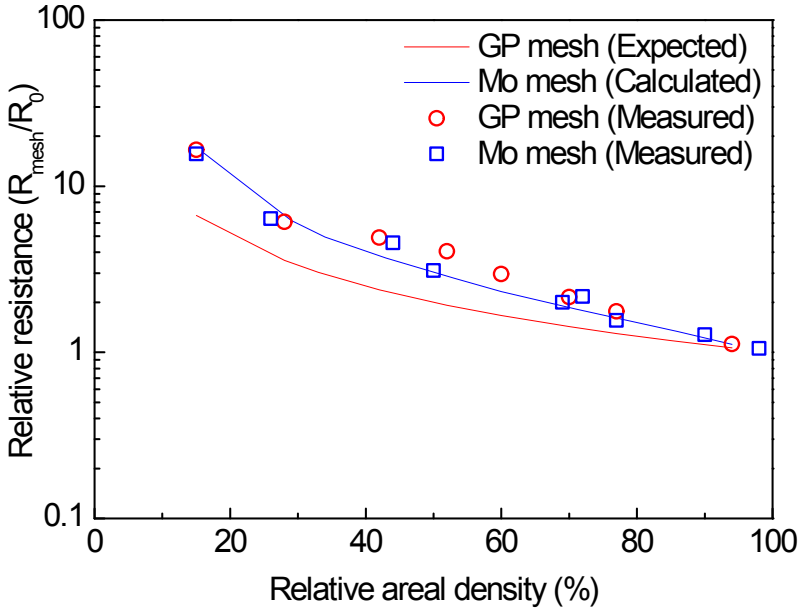

Fig. S4. The relative resistance change as a function of the relative areal density for a 2D molybdenum mesh and GP mesh. The expected result for the GP mesh is estimated by taking into consideration only the areal change, without the current flow disturbance in the neck region. In our FEM analysis, the current flow disturbance in the neck region of the mesh results in an additional increase in resistance. This indicates that the experimental result of the GP mesh is similar to that of the Mo mesh. Note that the nonlinear change with respect to the relative areal ratio is not associated with the material properties.

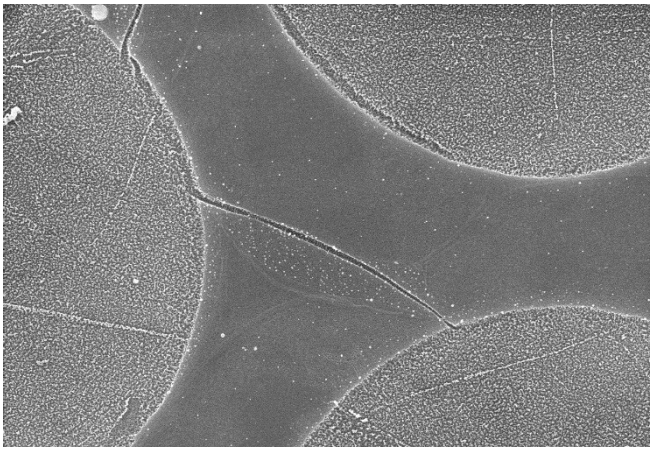

Fig. S5. Scanning electron microscopy (SEM) image showing defects in neck of the GP mesh. This graphene tear appears to occur during the transfer process, and when placed in the neck of the graphene mesh, the flow of current is cut off resulting in reduced conductivity.

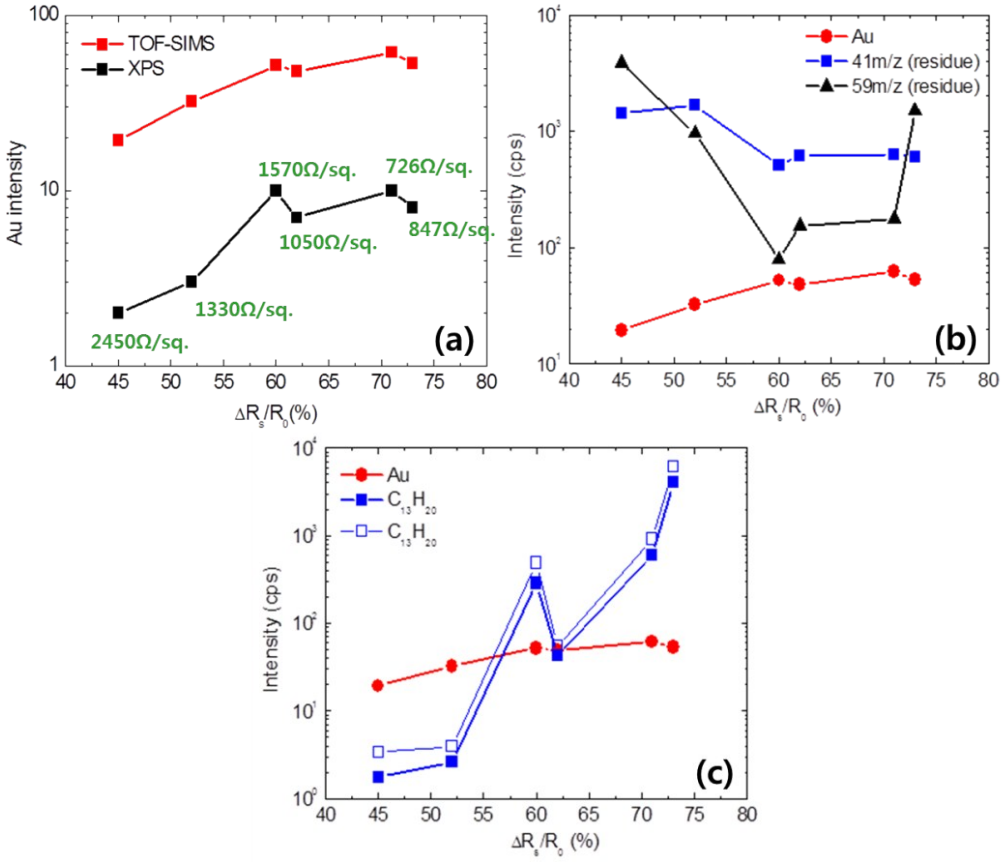

Fig. S6. (a) Comparison of the time-of-flight secondary ion mass spectrometry (ToF SIMS) and X-ray photoelectron spectroscopy (XPS) results as a function of the rate of resistance change. A large rate of resistance change implies that the sheet resistance can be decreased much more after doping of the GP mesh with $AuCl_3$. Moreover, the intensities of the signals corresponding to gold are increased in ToF SIMS and XPS, at lower sheet resistance values. (b) The relationship between the intensity of the signals corresponding to gold and the PR residues in ToF SIMS, as a function of the rate of resistance change. In ToF SIMS analysis, 41 m/z and 59 m/z are considered the main fragments of the PR residues. We observe that the 41 m/z fragment decreases as the rate of resistance change is increased. (c) The relationship between the signal intensity for the gold and the graphene fragments as a function of rate of the resistance

change. If the PR residues are effectively removed by washing with acetone, the intensity of the graphene fragment in ToF SIMS analysis is increased. Thus, gold nanoparticles can be effectively adsorbed on the exposed GP meshes, which results in a lower sheet resistance.

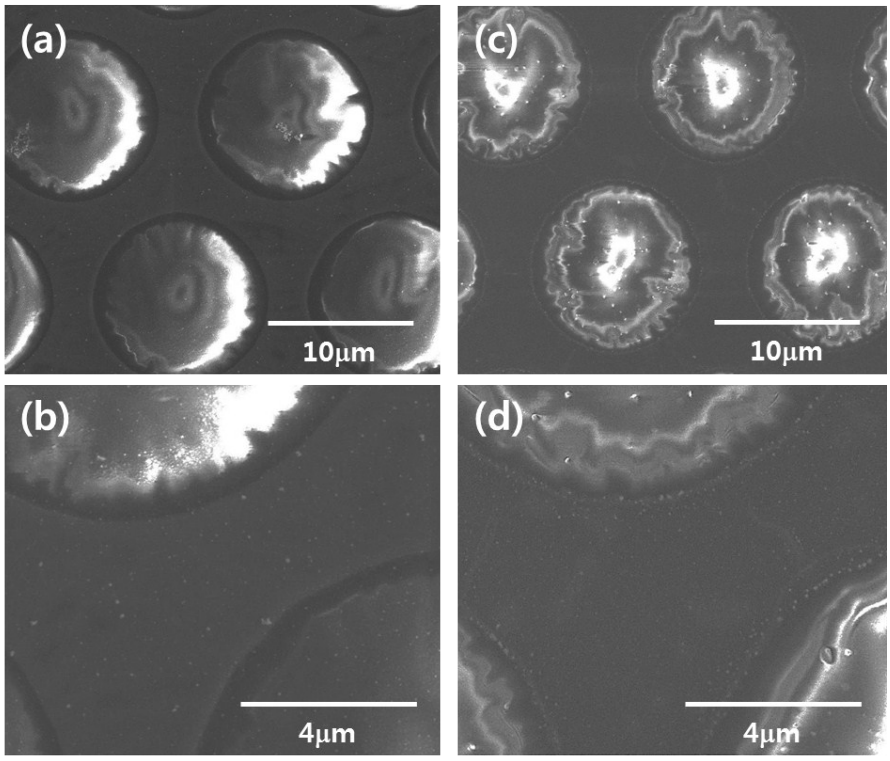

Fig. S7. (a) and (b) show the SEM images of the $AuCl_3$-doped GP mesh. (c) and (d) show the SEM images of the $AuCl_3$-doped GP mesh after electrical annealing. As the edges of the GP mesh are very active, the chemical materials including the dopants and PR residues can be easily adsorbed at this region. Through Joule heating in the electrical annealing process, the PR residues, which have been already adsorbed on the edge region of the GP mesh, can be effectively removed. Thus, the gold nanoparticles can be densely adsorbed on the surface and the edge region of the GP mesh, which results in a decreased sheet resistance.

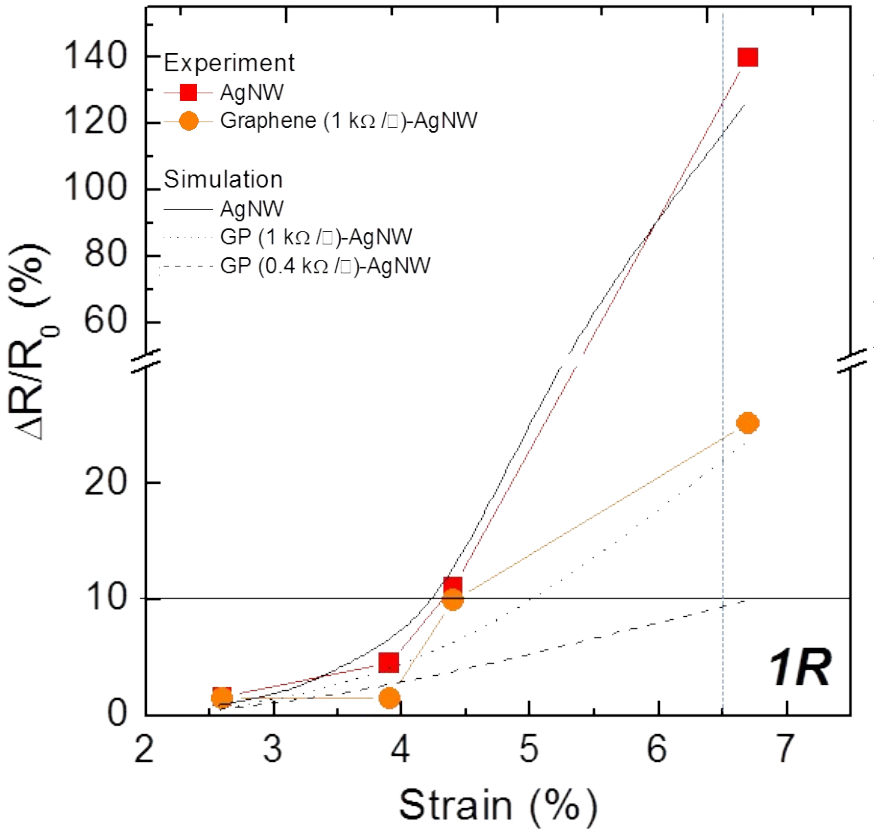

Fig. S8. Comparison of the changes in the resistances of the electrodes including the Ag nanowires and hybrid films, as a function of bending strain applied by varying the bending radius. The changes in the resistances compared to the initial resistances are finally estimated after in-situ resistance measurements over 20,000 cycles.

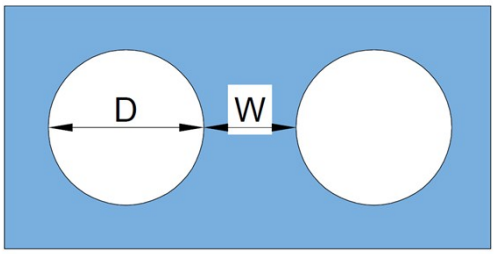

Photo-lithography					
L (mm)	W (μm)	D (μm)	N	L_E (m)	C_{Doping} (/cm^3)
20	2	8	2000.0	1.00E+02	5.83E+10
20	3	12	1333.3	6.70E+01	3.89E+10
20	4	16	1000.0	5.02E+01	2.91E+10
20	5	20	800.0	4.02E+01	2.33E+10
E-beam lithography					
L (mm)	W (nm)	D (nm)	N	L_E (m)	C_{Doping} (/cm^3)
20	100	400	40000	2.01E+03	1.17E+12
20	200	800	20000	1.00E+03	5.83E+11
20	400	1600	10000	5.02E+02	2.91E+11
20	1000	4000	4000	2.01E+02	1.17E+11

Table 1. T The calculated total edge length and doping concentration according to hole size and neck width in a 2 cm × 2 cm graphene mesh. The hole size was reduced from 20 μm to 400 nm while the ratio of D/W, in which the hole diameter is D and neck width is W, was maintained at 4. As the hole size decreases, the number of holes, N, in the graphene mesh of 2 cm × 2 cm increases in inverse proportion, and the total edge length, L_E, also increases in proportion to N ($L_E = D\pi N$). Here, the doping concentration is estimated assuming that the edge of the hole has an armchair structure and oxygen is bonded to the edge. As shown in the above table, the doing concentration is increased in proportion to the edge length.